Phase-stabilized electrically-driven microcomb

Thibault Wildi[1,†], Alexander E. Ulanov[1,†], Thibault Voumard[1], Bastian Ruhnke[1], Tobias Herr[1,2,*]

[1]Deutsches Elektronen-Synchrotron DESY, Notkestr. 85, 22607 Hamburg, Germany
[2]Physics Department, Universität Hamburg UHH, Luruper Chaussee 149, 22761 Hamburg, Germany
[†]These authors contributed equally
[*]tobias.herr@desy.de

Microresonator frequency combs (microcombs) hold potential for precision metrology in a compact form factor in applications such as point-of-care diagnostics, environmental monitoring, timekeeping, and navigation. Through the principle of self-injection locking, electrically-driven photonic chip-based microcombs with low complexity are now possible. Yet, phase-stabilization of such self-injection locked microcombs, a crucial property of metrological frequency combs, has been unattained. Here, addressing this critical need, we demonstrate full phase-stabilization of a self-injection locked microcomb. The microresonator is implemented in a silicon nitride photonic chip and by controlling a pump laser diode and a microheater with low voltage signals (sub 1.5 V), we achieve independent actuators for the comb's offset and line spacing frequencies. Both actuators reach a bandwidth of over 100 kHz and permit phase-locking to external frequency references. This establishes compact, electrically-driven photonic chip-based microcombs as scalable sources with low complexity for coherent precision metrology in emerging applications.

Optical frequency combs provide large sets of laser lines that are equidistant in optical frequency and mutually phase-coherent [1–3]. Owing to this property, they have enabled some of the most precise measurements in physics and are pivotal to a vast range of emerging applications from molecular sensing to geo-navigation. Now, frequency combs based on high-Q nonlinear optical microresonators (microcombs) [4, 5] can be fabricated in complementary metal–oxide–semiconductor (CMOS) compatible, [6, 7], low-cost, scalable wafer-scale processes, and promise to bring frequency comb technology into wide-spread application beyond optics laboratories [8–10]. In microcombs a continuous-wave (CW) driving laser with frequency ν_p is converted via nonlinear optical processes into a series of comb lines that are mutually spaced by the comb's repetition rate f_{rep}, so that $\nu_\mu = \nu_\mathrm{p} + \mu f_{\mathrm{rep}}$, describes the frequencies ν_μ in the comb ($\mu = 0, \pm1, ..$ is a mode index relative to the pump; see Fig. 1**c**). For many comb-based precision measurements, it is crucial to independently control the comb's defining parameters, here ν_p and f_{rep}, on a level that permits full phase control, i.e. *phase-locking* of ν_p and f_{rep} to external frequency references. For instance, this is important for environmental monitoring, medical diagnostics, geo-navigation, searches for exo-planets, and other emerging applications that rely on phase-coherent links between electromagnetic waves.

A major advancement in microcombs came through the principle of self-injection locking (SIL) [11–13], which enabled electrically-driven integrated comb generators with drastically reduced operational complexity [14, 15] and additional chip-level integration [16–20]. Instead of a low-noise table-top pump laser, SIL leverages a narrow linewidth injection feedback from the high-Q microresonator to a chip-scale semiconductor pump laser. The SIL mechanism leads to a low-noise pump laser and elegantly ensures that the laser is intrinsically tuned to the resonator for comb generation. Although extremely attractive, the simplicity and compactness of SIL-based combs entails a critical flaw with regard to controlling ν_p and f_{rep}. In contrast to previous table-top systems that utilized the driving laser frequency and the driving laser power (heating of the resonator) as independent actuators to stabilize ν_p and f_{rep} [21], these parameters are not independent in SIL-based systems (both depend on the laser pump current). Moreover, in a SIL-based system, there exists a feedback from the resonator to the driving laser frequency that is absent in previous demonstrations, resulting in non-trivial dynamics [20]. Until now, only the stabilization of one degree of freedom (f_{rep}) has been demonstrated [22]. The lack of full-phase stabilization represents a serious shortcoming of SIL microcombs.

Here, we demonstrate a fully phase-stabilized chip-scale electrically-driven microcomb. The comb is based on the SIL principle and benefits from synthetically generated back-reflection for deterministic and robust SIL operation [23]. In addition to the laser pump current, we utilize an integrated electric microheater as a second independent actuator. Both actuators achieve effective locking bandwidth of more than 100 kHz and permit robust phase-locking of ν_p and f_{rep}. Importantly, unlike alterna-

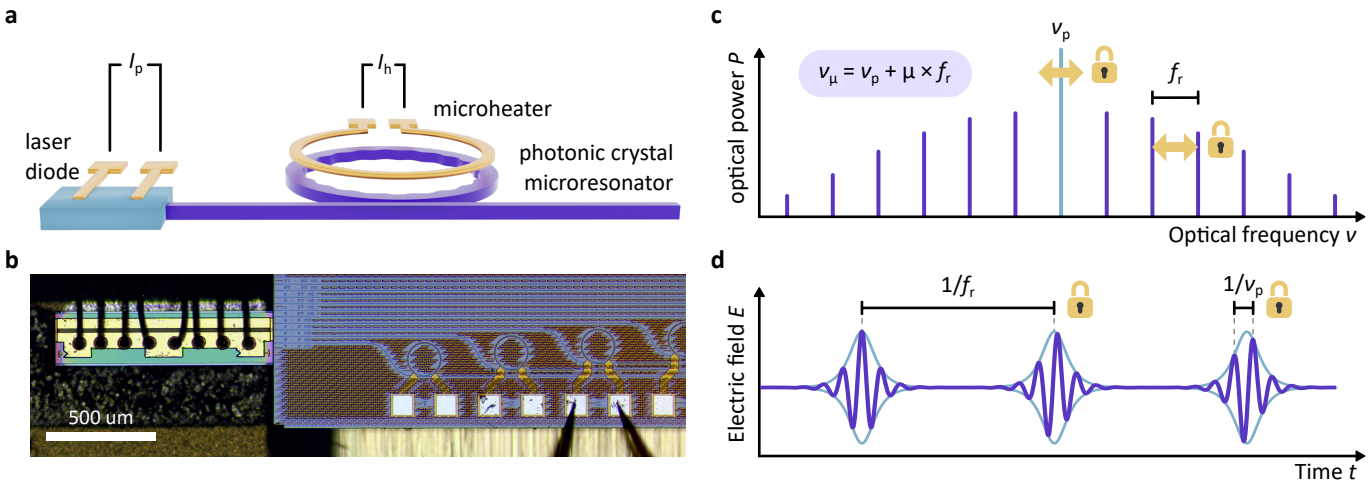

Figure 1 | **Phase-stabilized electrically-driven microcomb**. **a**, Synthetic-reflection self-injection-locked (SIL) microcombs are turn-key optical frequency comb sources. The combined actuation of the laser diode current I_p and the current I_h of a microheater controlling the microring temperature enables full-phase stabilization of the microcomb with low CMOS-compatible voltages, all within a millimeter-scale platform. **b**, Micrograph of the SIL microcomb source comprised of a DFB laser diode (left) butt-coupled to a Si_3N_4 microresonator (right). A metallic microheating element embedded in the SiO_2 cladding is routed above the microring. **d**, **c**, The optical spectrum of a continuous-wave driven microcomb is comprised of equidistant lines ν_μ spaced by the comb's repetition rate f_rep and centered on the pump frequency ν_p. Full phase stabilization of the microcomb entails locking both degrees of freedom to an external reference, which corresponds in the time domain, to a pulse train with a stabilized period $\tau = 1/f_\mathrm{rep}$ and optical carrier frequency.

tive high-voltage piezo-electric or electro-optic actuators, our system requires for operation only low voltages below 1.5 V (CMOS-compatible). Thus, our approach aligns with critical requirements of chip-integrated technologies.

Setup

The experimental setup for stabilization of the SIL microcomb is shown in Fig. 2**a**. In our work, the SIL microcomb source is based on dissipative Kerr-solitons (DKS) [5, 8, 24] in a continuous-wave (CW) laser-driven photonic-chip integrated silicon nitride ring with nano-corrugated side-walls (photonic crystal ring resonator, PhCR) [23, 25–27]. The microresonator is characterized by a free spectral range of 300 GHz, anomalous group velocity dispersion, and a high quality factor $Q \approx 1.5 \times 10^6$ (see Methods for more details). An integrated metallic microheater is embedded in the silica cladding, 1.7 µm above the resonator waveguide. The photonic chip is butt-coupled to a semiconductor distributed feedback (DFB) CW laser diode delivering approximately 25 mW of on-chip optical pump power at 1557 nm. Our system leverages a recently demonstrated synthetic reflection technique [23], where the nano-patterned corrugation of the PhCR generates tailored optical feedback for robust self-injection locking of the driving laser diode, also forcing exclusive and deterministic single-soliton operation [25]. Importantly, synthetic reflection can substantially extend the range of pump frequency-to-resonance detuning accessible via SIL, resulting in an increased overlap between the SIL operation and the DKS existence ranges. This is beneficial for phase-coherent stabilization of self-injection-locked microcombs as it allows for a large actuation range of the driving laser frequency while remaining in SIL operation [23].

The generated microcomb is outcoupled from the chip through a cleaved ultra-high numerical aperture (UHNA-7) optical fiber using index-matching gel to minimize unwanted back-scattering at the chip facet. Once the temperature and injection phase are appropriately adjusted (the DFB laser and microresonator dies are actively and independently temperature-stabilized), the system deterministically enters single-DKS operation when the laser diode current is set to a predetermined setpoint ∼180 mA (∼1.42 V). Fig. 2**c** shows the resulting microcomb spectrum, with a FWHM of 1.44 THz and a total power of 10 mW.

In SIL DKS operation, the DFB laser's emission frequency ν_p (the central comb line of the microcomb) can be tuned by adjusting the current around the setpoint with a sensitivity of 27 MHz mA^{-1}, which also affects the DKS repetition rate by 160 kHz mA^{-1}. A second degree of freedom is provided by the resonator's microheater, which we operate at a current bias of 3 mA (105 mV). Remarkably, this corresponds to a power consumption of only 315 µW. Via the microheater, the microcomb's repetition rate f_rep can be tuned with a sensitivity of ∼400 kHz mA^{-1}. As the laser diode and the microresonator are coupled through SIL, the microheater also induces a shift in the microcomb's center frequency ν_p (pump line) with a sensitivity of ∼160 MHz mA^{-1}. The actuator sensitivities are summarized in Table 1. As the corresponding control matrix is diagonalizable with non-zero diagonal elements, the two actuators enable independent control of both degrees of freedom of the SIL microcomb (ν_p and f_rep).

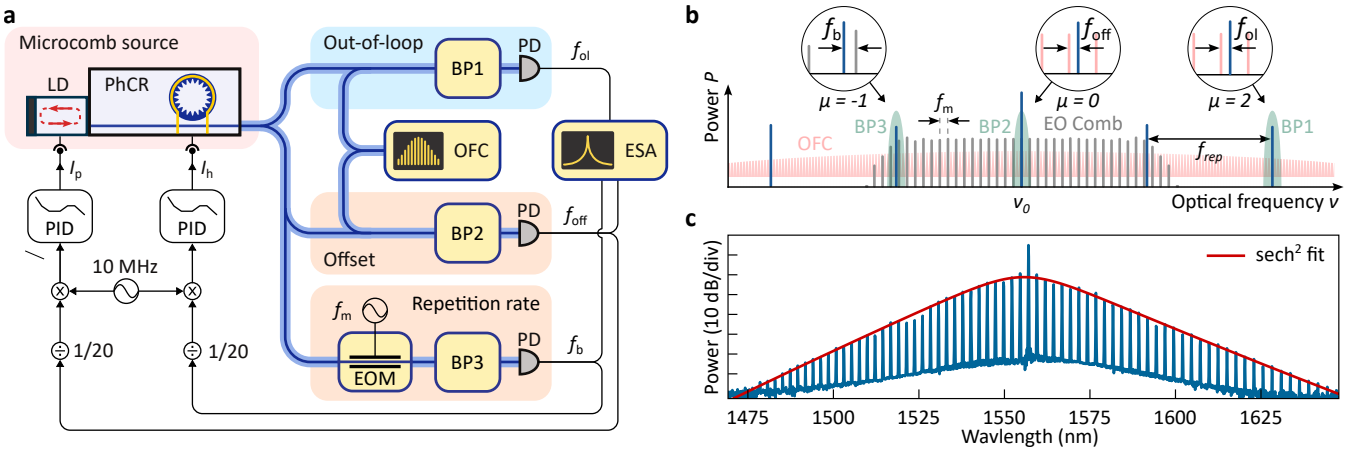

Figure 2 | **Experimental setup**. **a**, The microcomb source, a laser diode self-injection-locked to a PHCR operating in the DKS regime, is stabilized via the actuation of the diode and heater currents. OFC: reference optical frequency comb ESA; electronic spectrum analyzer; EOM: electro-optic modulator; BP: bandpass filter; PD: photodetector; LD: laser diode; PhCR: photonic crystal resonator; PID: proportional-integral-derivative controller. **b**, Frequency diagram, depicting the SIL microcomb (blue), the reference 1 GHz oscillator (red) and the electro-optic modulation comb (grey). The frequencies f_b, f_{off}, and f_{ol}, corresponding to the repetition rate, offset, and out-of-loop beat notes, respectively, are extracted by the optical bandpass filters BP1-3 (green) as shown in the insets. **c**, Optical spectrum of self-injection-locked microcomb. The spectrum is well fitted by a sech^2 envelope with a FWHM of 1.44 THz.

To demonstrate phase-coherent stabilization as well as to provide an out-of-loop validation, we utilize a conventional optical frequency comb (OFC) as a reference, whose repetition rate of 1 GHz is stabilized to the 10 MHz signal from a GPS disciplined Rb-clock. The error signal for stabilization of ν_p is generated by combining a fraction of the microcomb light with that from the reference OFC. An optical bandpass filter (BP2) is used to isolate the beat note f_{off} between the microcomb's central line and the closest line of the reference OFC (see Fig. 2**b**) [21, 28]. To obtain the repetition rate error signal, we utilize electro-optic phase-modulation (modulation frequency $f_m \approx 17.5$ GHz) of the central comb line and detect the beating $f_b = f_{rep} - 17 \times f_m \approx 200$ MHz between 17th modulation sideband and the first sideband of the microcomb [29]. Both beat notes are then frequency-divided down to approximately 10 MHz, and the error signals are extracted through phase detection with respect to the 10 MHz reference oscillator (all microwave sources and recording devices are also referenced to the 10 MHz signal from the Rb-clock). The phase-lock loops (PLLs) are implemented using two proportional-integral-derivative (PID) controllers, acting onto the SIL laser driving current and resonator microheater current for the offset and repetition rate stabilization, respectively. As follows from Table 1, alternative configurations of the PLLs are possible, e.g., switching the actuators or simultaneously using both actuators for both degrees of freedom to diagonalize the control matrix.

Sensitivity	f_{off}	f_{rep}
I_p	27 MHz/mA	160 kHz/mA
I_h	160 MHz/mA	400 kHz/mA

Table 1 | **Actuator sensitivity**. Sensitivity of the SIL microcomb's offset frequency f_{off} and repetition rate f_{rep} to the DFB current I_p and micro-heater current I_h. The values were measured around the experiment setpoint of ∼180 mA and 3 mA, respectively.

Finally, an out-of-loop (OL) measurement of the microcomb's phase-stability is obtained by recording the beat note $f_{ol} = 2 \times f_{rep} + f_{off} - m \times 1$ GHz between the second sideband of the microcomb and the m^{th} sideband of the reference oscillator. With contributions from both locks, this is a key metric in evaluating the overall system performance.

Experiments

The successive initiation of both PLLs is shown in Fig. 3**a** where the spectrogram of the out-of-loop beat note is presented. While the offset lock already significantly enhances the stability of the out-of-loop beat note (∼1.75 s), residual fluctuations of the microcomb's repetition rate f_{rep} are only suppressed with the initiation of the repetition rate lock (∼2.8 s) resulting in a fully phase-stabilized system. Thus, the independence of both high-bandwidth actuators and the extended detuning range reliably obtained through synthetic reflection enables robust phase stabilization of the microcomb.

Next, we study the long-term stability of our source in the fully phase-locked state by recording each second the frequency counts of the out-of-loop beat note with a gate time $\tau = 1$ s (the counts are extracted from the signal's quadratures, see Methods). The measured counts are displayed in Fig. 3**b** and the corresponding histogram is presented in Fig. 3**c** (standard deviation of 4.25 Hz). We also acquire analogous data for the offset and repetition rate in-loop beat note signals when the microcomb is fully phase-locked. All three datasets are processed to

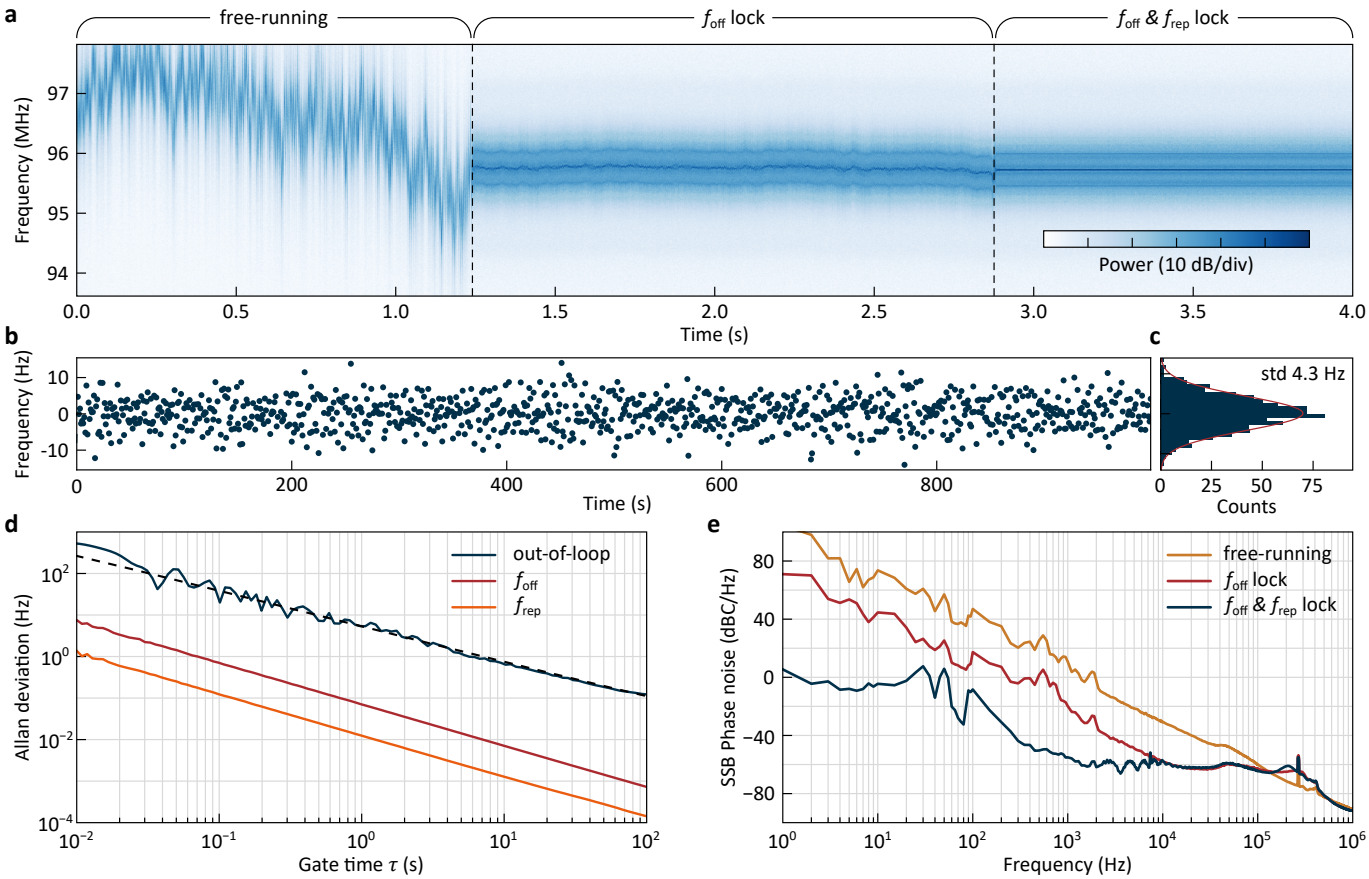

Figure 3 | **Full phase stabilization of the SIL microcomb**. **a**, Spectrogram of the out-of-loop beat note f_{ol} showing the transition from a free-running to a fully-locked state through the successive initiation of the offset and repetition rate locks. **b**, Time series measurement of the out-of-loop frequency f_{oll} in the fully-locked state. The samples are acquired using a 1 s gate time at a rate of 1 Hz. **c**, Histogram of the values shown in **b**; well as Gaussian distribution with a standard deviation (std) of 4.3 Hz. **d**, Overlapping Allan deviation of the out-of-loop signal (blue) and two in-loop signals (red - offset frequency, orange - microcomb repetition rate). Exponential fits are shown as dashed lines and scale with the gate time τ as $\tau^{-0.823}$, $\tau^{-0.996}$ and $\tau^{-0.990}$ respectively. The frequency counter noise floor, 40 dB below the level of f_{rep}, is not shown. **e**, Phase noise (solid lines, left axis) of the out-of-loop beat note f_{ol} in the free-running (orange), offset-locked (red) and fully-locked states (blue).

extract the overlapping Allan deviation (OAD) presented in Fig. 3**d** (see Methods). The OAD of the in-loop signals averages down with $\tau^{-0.996}$ and $\tau^{-0.990}$ while that of the out-of-loop signal scales with $\tau^{-0.823}$. The latter value differs from the τ^{-1} scaling expected from a phase-lock with zero-phase fluctuation due to slow environmental fluctuations (e.g., lab air conditioning); however, we emphasize that the PLLs keep the phase fluctuation much smaller than π, hence providing a robust phase lock. The footprint of our system (sub-1 mm^2 without electronics), as well as its cost and complexity, are orders of magnitude below previous phase-stabilized microcombs that relied on table-top lasers, amplifiers, and high-voltage actuators.

The phase noise of the out-of-loop beat note in the free-running, offset-locked, and fully-locked states is shown in Fig. 3**e**. In the fully locked state, at frequencies below 1 kHz, the OL phase noise is limited by the digital PLL stabilizing the reference oscillator [30].

The closed-loop frequency response of the repetition rate and offset phase-lock loops are shown in Fig. 4**a** and **b** respectively (with the respective other degree of freedom unlocked). Notably, a bandwidth over 100 kHz and 300 kHz respectively is achieved for the microheater-based repetition rate actuator and the laser diode-based offset actuator. The actuators allow for broadband noise suppression, as can be observed from the SSB phase noise of the repetition rate and offset signals (Fig. 4**c** and **d**) and their corresponding beat notes (Fig. 4**e** and **f**). Notably, despite cross-talk between the two PLLs, no significant degradation of the locks is observed in the fully locked state.

Conclusion

In conclusion, we demonstrate full phase-stabilization of self-injection-locked microresonator frequency comb. Based on a photonic-chip integrated microresonator, our system does not employ electro- or acoustic-optic mechanisms and relies solely on CMOS-compatible driving and control voltages. Excluding electronics, the entire system

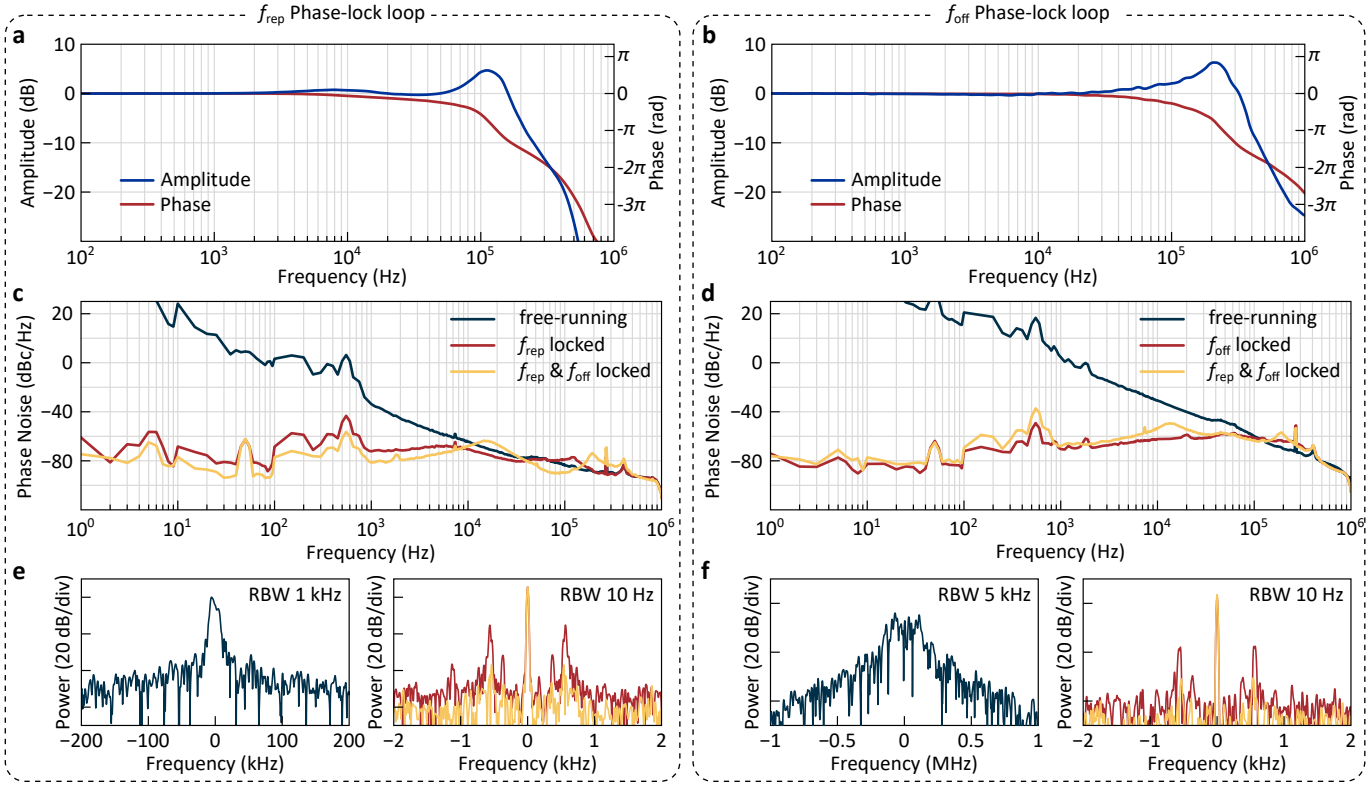

Figure 4 | **Phase-lock loops**. **a**, **b**, Close-loop frequency response of the repetition rate (**a**) and offset frequency (**b**) phase-lock loops. **c**, **d**, SSB phase noise of f_{rep} (**a**) and f_{off} (**b**) in the free-running, partially locked and fully-locked states. **e**, **f**, repetition rate beat notes (**e**) and offset beat notes (**f**) corresponding to the respective state shown in **c** and **d**. Note the difference in scale of the frequency axis between the free-running (left) and locked (right) states.

is implemented in

The microcomb's offset frequency is controlled using DFB laser diode injection current, while on-chip metallic heaters stabilize the repetition rate. Both actuators feature a bandwidth over 100 kHz and operate simultaneously without noticeable detrimental effects from cross-coupling. In conjunction with synthetic reflection self-injection locking, this configuration enables complete phase locking of the microcomb's defining parameters. These findings position self-injection locked microcombs as valuable assets for coherent frequency metrology in portable and compact systems.

Methods

Sample fabrication. The samples were fabricated commercially by LIGENTEC SA using ultraviolet stepper optical lithography. A microresonator ring radius of 75 µm was chosen, corresponding to a free-spectral range (FSR) of 300 GHz, while a waveguide width of 1600 nm and a waveguide height of 800 nm provide anomalous group-velocity dispersion (difference between neighboring FSRs, $D_2 \approx 9$ MHz). Synthetic feedback to the driving DFB diode laser is provided by a nano-patterned corrugation with a peak-to-peak amplitude of 4 nm and a period $2\pi/(2m_0)$, where $m_0 = 550$ is the azimuthal mode number to which the pump diode is coupled, corresponding to wavelength of ∼1557 nm. The corrugation leads to a forward-backward coupling rate $\gamma/(2\pi) = 145$ MHz. For all modes, including the pump mode, a high quality factor $Q \approx 1.5 \times 10^6$ is achieved.

Frequency stability measurements. To measure the long-term stability of our microwave signals, we record the beat note's in-phase and quadrature (IQ) components using the built-in IQ-analyzer of our electronic spectrum analyzer (Rohde & Schwarz FSW26). The phase is then extracted from the IQ data, from which the overlapping Allan deviation is computed using the *AllanTools* python module implementing the NIST standards [31]. Frequency counts are obtained by suitably differentiating the extracted phase. Spectrograms, spectra, and phase noises are similarly calculated from IQ data, allowing for greater versatility and post-acquisition adjustment of the resolution bandwidth, video bandwidth, and associated windowing functions.

Author Contributions

T.W., A.U., and T.H. conceived the experiment. T.W. and A.U. designed the setup and the photonic chip, performed the experiments, and analyzed the data. T.V. developed and operated the reference comb. B.R. supported the design of the resonator and the experiments. T.H. supervised the work. T.W., A.U., and T.H. prepared the manuscript with input from all authors.

Funding

This project has received funding from the European Research Council (ERC) under the EU's Horizon 2020 research and innovation program (grant agreement No 853564), from the EU's Horizon 2020 research and innovation program (grant agreement No 965124) and through the Helmholtz Young Investigators Group VH-NG-1404; the work was supported through the Maxwell computational resources operated at DESY.

Disclosures

All authors declare no conflict of interest.

References

1. Cundiff, S. T. *Colloquium*: Femtosecond Optical Frequency Combs. *Reviews of Modern Physics* **75,** 325–342 (2003).
2. Fortier, T. & Baumann, E. 20 Years of Developments in Optical Frequency Comb Technology and Applications. *Communications Physics* **2,** 1–16 (2019).
3. Diddams, S. A., Vahala, K. & Udem, T. Optical Frequency Combs: Coherently Uniting the Electromagnetic Spectrum. *Science* **369,** eaay3676 (2020).
4. Del'Haye, P. *et al.* Optical Frequency Comb Generation from a Monolithic Microresonator. *Nature* **450,** 1214–1217 (2007).
5. Herr, T. *et al.* Temporal Solitons in Optical Microresonators. *Nature Photonics* **8,** 145–152 (2014).
6. Levy, J. S. *et al.* CMOS-compatible Multiple-Wavelength Oscillator for on-Chip Optical Interconnects. *Nature Photonics* **4,** 37–40 (2010).
7. Brasch, V. *et al.* Photonic Chip–Based Optical Frequency Comb Using Soliton Cherenkov Radiation. *Science* **351,** 357–360 (2016).
8. Kippenberg, T. J., Gaeta, A. L., Lipson, M. & Gorodetsky, M. L. Dissipative Kerr Solitons in Optical Microresonators. *Science* **361** (2018).
9. Gaeta, A. L., Lipson, M. & Kippenberg, T. J. Photonic-Chip-Based Frequency Combs. *Nature Photonics* **13,** 158–169 (2019).
10. Pasquazi, A. *et al.* Micro-Combs: A Novel Generation of Optical Sources. *Physics Reports. Micro-Combs: A Novel Generation of Optical Sources* **729,** 1–81 (2018).
11. Vasil'ev, V. V. *et al.* High-Coherence Diode Laser with Optical Feedback via a Microcavity with 'whispering Gallery' Modes. *Quantum Electronics* **26,** 657 (1996).
12. Liang, W. *et al.* Whispering-Gallery-Mode-Resonator-Based Ultranarrow Linewidth External-Cavity Semiconductor Laser. *Optics Letters* **35,** 2822–2824 (2010).
13. Kondratiev, N. M. *et al.* Recent Advances in Laser Self-Injection Locking to High-Q Microresonators. *Frontiers of Physics* **18,** 21305 (2023).
14. Liang, W. *et al.* High Spectral Purity Kerr Frequency Comb Radio Frequency Photonic Oscillator. *Nature Communications* **6,** 7957 (2015).
15. Pavlov, N. G. *et al.* Narrow-Linewidth Lasing and Soliton Kerr Microcombs with Ordinary Laser Diodes. *Nature Photonics* **12,** 694–698 (2018).
16. Stern, B., Ji, X., Okawachi, Y., Gaeta, A. L. & Lipson, M. Battery-Operated Integrated Frequency Comb Generator. *Nature* **562,** 401 (2018).
17. Raja, A. S. *et al.* Electrically Pumped Photonic Integrated Soliton Microcomb. *Nature Communications* **10,** 680 (2019).
18. Shen, B. *et al.* Integrated Turnkey Soliton Microcombs. *Nature* **582,** 365–369 (2020).
19. Xiang, C. *et al.* High-Performance Lasers for Fully Integrated Silicon Nitride Photonics. *Nature Communications* **12,** 6650 (2021).
20. Voloshin, A. S. *et al.* Dynamics of Soliton Self-Injection Locking in Optical Microresonators. *Nature Communications* **12,** 235 (2021).
21. Del'Haye, P., Arcizet, O., Schliesser, A., Holzwarth, R. & Kippenberg, T. J. Full Stabilization of a Microresonator-Based Optical Frequency Comb. *Physical Review Letters* **101,** 053903 (2008).
22. Ji, Q.-X. *et al.* Engineered Zero-Dispersion Microcombs Using CMOS-ready Photonics. *Optica* **10,** 279–285 (2023).
23. Ulanov, A. E. *et al. Synthetic-Reflection Self-Injection-Locked Microcombs* 2023. arXiv: `2301.13132 [physics]`.
24. Leo, F. *et al.* Temporal Cavity Solitons in One-Dimensional Kerr Media as Bits in an All-Optical Buffer. *Nature Photonics* **4,** 471–476 (2010).
25. Yu, S.-P. *et al.* Spontaneous Pulse Formation in Edgeless Photonic Crystal Resonators. *Nature Photonics* **15,** 461–467 (2021).
26. Lucas, E., Yu, S.-P., Briles, T. C., Carlson, D. R. & Papp, S. B. Tailoring Microcombs with Inverse-Designed, Meta-Dispersion Microresonators. *Nature Photonics* **17,** 943–950 (2023).
27. Moille, G., Lu, X., Stone, J., Westly, D. & Srinivasan, K. Fourier Synthesis Dispersion Engineering of Photonic Crystal Microrings for Broadband Frequency Combs. *Communications Physics* **6,** 1–11 (2023).
28. Jost, J. D. *et al.* Counting the Cycles of Light Using a Self-Referenced Optical Microresonator. *Optica* **2,** 706–711 (2015).
29. Del'Haye, P., Papp, S. B. & Diddams, S. A. Hybrid Electro-Optically Modulated Microcombs. *Physical Review Letters* **109,** 263901 (2012).

30. Voumard, T. *et al.* 1-GHz Dual-Comb Spectrometer with High Mutual Coherence for Fast and Broadband Measurements. *Optics Letters* **47,** 1379–1382 (2022).

31. Riley, W. & Howe, D. *Handbook of Frequency Stability Analysis* 2008.